<center>Electronic Supporting Information</center>

Unravelling the Photophysics of Triphenylamine and Diphenylamine Dyes: A Comprehensive Investigation with *ortho-*, *meta-* and *para-* Amido Substituted Derivatives

Narendra Mandare[a,#], Ponnusamy Shanmugam[b] Mahesh Sundararajan[c], and Sharmistha Dutta Choudhury[a,d,*]

[a]Radiation & Photochemistry Division, Bhabha Atomic Research Centre, Mumbai 400085, India.

[b]Organic and Bio-Organic Chemistry Division, CSIR-Central Leather Research Institute, Adyar, Chennai-600020, India; and Professor of Chemistry at the Academy of Scientific and Innovative Research (AcSIR), Anusandhan Bhawan, 2, Rafi Marg, New Delhi, India.

[c]Theoretical Chemistry Section, Bhabha Atomic Research Centre, Mumbai 400085, India

[d]Homi Bhabha National Institute, Training School Complex, Anushaktinagar, Mumbai 400094, India.

[#]On M.Sc. project from K. J. Somaiya College of Science and Commerce, Mumbai, India.

Corresponding Author:

*E-mail: sharmidc@barc.gov.in; Telephone: 91-22-25595101; Fax: 91-22-25505151

Note S1. Synthesis and Characterization of the DPA and TPA derivatives

The DPA and TPA series of dyes were synthesized by N-mono and N,N-diarylation of various positionally placed aminobenzamides, using benzyne, as described in a previous publication.[1] Briefly, 2-, 3- or 4-aminobenzamide was reacted with benzyne, which was generated *in situ* from 2.2 equivalents of 2-(trimethylsilyl) phenyl trifluoromethane sulfonate using 4 equivalents of KF and 18-crown 6, in dry acetonitrile under Ar atmosphere at RT. The typical reaction scheme yielding both mono- and di- arylated products in excellent combined yield is shown in Chart S1. The product mixture was purified by silica gel column chromatography to obtain the pure compounds (DPA-*o* and TPA-*o*, DPA-*m* and TPA-*m*, DPA-*p* and TPA-*p*), which were subsequently characterised by spectroscopic techniques.
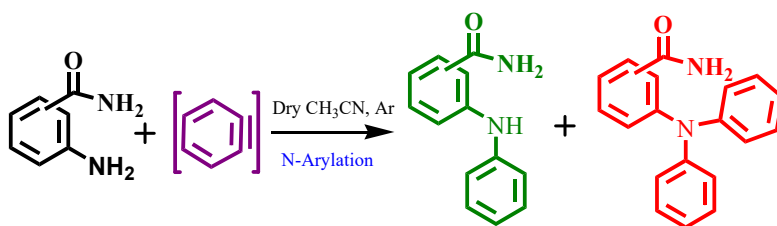
Chart S1. General scheme for the synthesis of *N*-mono (DPA series) and *N,N*-diarylated (TPA series) derivatives from 2-, 3- or 4-aminobenzamide.

2-(Diphenylamino)benzamide (TPA-*o*). Colourless crystals; R_f (30% EtOAc-hexane): 0.40; FTIR (KBr) λ_{max}: 3421, 3328, 3242, 3134, 3030, 2923, 2854, 1945, 1671, 1588, 1486, 1448, 1373, 1278, 1247, 1153, 1082, 1035, 970, 919, 880, 820, 783, 752, 694, 621, 509 cm^{-1}; ^{1}H NMR (400 MHz, CDCl$_3$): δ 7.94 (dd, J = 7.8, 1.3 Hz, 1H), 7.40 (td, J = 7.8, 1.5 Hz, 1H), 7.25 (t, J = 7.6 Hz, 2H), 7.17 (dd, J = 12.7, 4.3 Hz, 4H), 7.07 (d, J = 7.9 Hz, 1H), 6.93 (t, J = 8.9 Hz, 6H), 5.58 (s, 1H); ^{13}C NMR (CDCl$_3$/TMS, 100 MHz): δ 121.5, 122.4, 123.0, 126.1, 129.3, 129.4, 130.3, 131.7, 132.8, 145.1, 147.4, 168.0; HRMS-ESI: calculated for C$_{19}$H$_{16}$N$_2$O [M]$^+$ m/z: 288.1063; found 288.0989.

3-(Diphenylamino)benzamide (TPA-*m*). Yellowish powder; R_f (30% EtOAc-hexane): 0.48; FTIR (KBr) λ_{max}: 3521, 3429, 3343, 3235, 3132, 2943, 2854, 1845, 1691, 1488, 1448, 1353, 1298, 1237, 1143, 1052, 1035, 919, 862, 820, 762, 752, 684, 621, 506 cm^{-1}; ^{1}H NMR (400 MHz, CDCl$_3$): δ 7.43 (t, J = 1.9 Hz, 1H), 7.31−7.28 (m, 1H), 7.21−7.10 (m, 6H), 7.01−6.93 (m, 6H), 6.06 (s, 2H); ^{13}C NMR (CDCl$_3$/TMS, 100 MHz): δ 120.9, 122.0, 123.4, 124.5, 126.7, 129.4, 134.7, 147.3, 148.4, 169.5; HRMS-ESI: calculated for C$_{19}$H$_{16}$N$_2$O [M]$^+$ m/z: 288.1063; found 289.1141.

4-(Diphenylamino)benzamide (TPA-*p*). Yellowish powder; R_f (30% EtOAc-hexane): 0.46; FTIR (KBr) λ_{max}: 3411, 3458, 3422, 3314, 3200, 2973, 2844, 1845, 1761, 1658, 1448, 1353, 1228, 1156, 1072, 1055, 960, 919, 860, 822, 773, 752, 674, 623, 509 cm^{-1}; ^{1}H NMR (400 MHz, CDCl$_3$): δ 7.59−7.56 (m, 2H), 7.24−7.20 (m, 4H), 7.07−7.01 (m, 6H), 6.95−6.93 (m, 2H), 5.83 (s, 2H); ^{13}C NMR (CDCl$_3$/TMS, 100 MHz): δ 120.6, 124.2, 125.3, 125.6, 128.6, 129.5, 146.8, 151.3, 168.9; HRMS-ESI: calculated for C$_{19}$H$_{16}$N$_2$O [M]$^+$ m/z: 288.1063; found 289.1106.
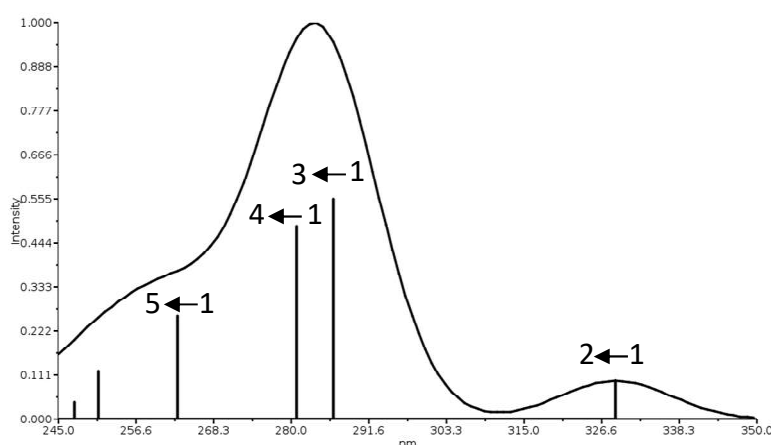
2-(Phenylamino)benzamide (DPA-*o*). Colourless powder; R_f (30% EtOAc-hexane): 0.42; FTIR (KBr) λ_{max}: 3454, 3416, 3339, 3169, 2885, 2735, 1623, 1585, 1513, 1443, 1391, 1316, 1289, 1158, 1078, 889, 743, 693, 625, 560, 500 cm^{-1}; ^{1}H NMR (400 MHz, CDCl$_3$): δ 9.43 (s, 1H), 7.39 (dd, J = 7.9, 1.4 Hz, 1H), 7.28−7.17 (m, 4H), 7.15−7.12 (m, 2H), 6.98−6.93 (m, 1H), 6.67 (ddd, J = 8.1, 6.9, 1.4 Hz, 1H), 5.92 (s, 2H); ^{13}C NMR (CDCl$_3$/TMS, 100 MHz): δ 115.3, 116.0, 117.5, 121.5, 122.8, 128.3, 129.3, 132.9, 141.2, 146.9, 171.9; HRMS-ESI: calculated for C$_{13}$H$_{12}$N$_2$O [M + H]$^+$ m/z: 213.0910, found 213.0892.

3-(Phenylamino)benzamide (DPA-*m*). Colourless powder; R_f (30% EtOAc-hexane): 0.43; FTIR (KBr) λ_{max}: 3453, 3420, 3343, 3201, 2885, 2363, 1657, 1598, 1521, 1416, 1378, 1303, 1289, 1258, 1063, 788, 653, 615, 560 cm^{-1}; ^{1}H NMR (400 MHz, CDCl$_3$): δ 7.44−7.43 (m, 1H), 7.25−7.18 (m, 4H), 7.17−7.12 (m, 2H), 7.04−7.01 (m, 2H), 6.91 (t, J = 7.4 Hz, 1H), 5.91

(s, 2H); ^{13}C NMR (CDCl$_3$/TMS, 100 MHz): δ 114.0, 115.9, 116.1, 118.8, 118.9, 120.2, 122.0, 123.5, 124.0, 124.6, 129.5, 134.5, 139.2, 142.1, 144.0, 169.6; HRMS-ESI: calculated for C$_{13}$H$_{12}$N$_2$O [M + H]$^+$ m/z: 213.0910, found 213.0862.

4-(Phenylamino)benzamide (DPA-*p*). Colourless powder; R$_f$ (30% EtOAc-hexane): 0.40; FTIR (KBr) λ$_{max}$: 3553, 3473, 3343, 2976, 2635, 2360, 1652, 1554, 1501, 1444, 1388, 1329, 1279, 1248, 1043, 712, 623, 625, 573 cm^{-1}; ^{1}H NMR (400 MHz, CDCl3): δ 7.66−7.62 (m, 2H), 7.28−7.23 (m, 2H), 7.09 (ddd, J = 3.0, 2.5, 1.4 Hz, 2H), 7.00−6.92 (m, 3H), 5.98 (s, 1H), 5.74 (s, 2H); ^{13}C NMR (CDCl$_3$/TMS, 100 MHz): δ 115.0, 120.1, 122.9, 124.1, 129.2, 129.5, 141.0, 147.3, 168.9; HRMS-ESI: calculated for C$_{13}$H$_{12}$N$_2$O [M + H]$^+$ m/z: 213.0910, found 213.0892.

(A)

(B)

(1) HOMO

(2) LUMO   (3) LUMO+1   (4) LUMO+2   (4) LUMO+3
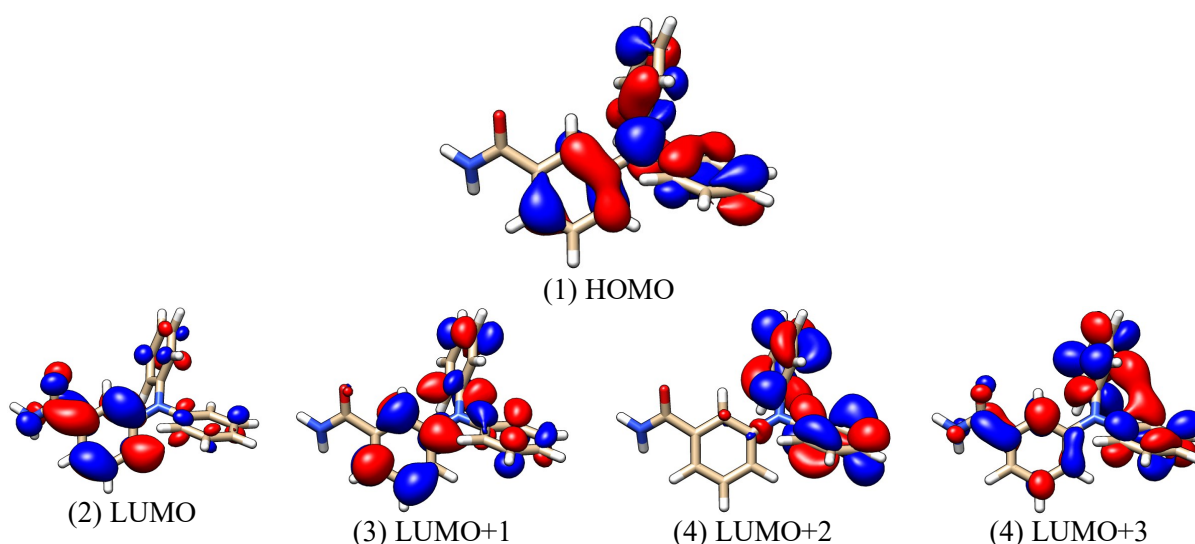
Fig. S1. (A) Computed absorption spectrum of TPA-*m* dye considering ACN as the solvent medium. (B) Molecular orbitals involved in the four lowest transitions are shown.
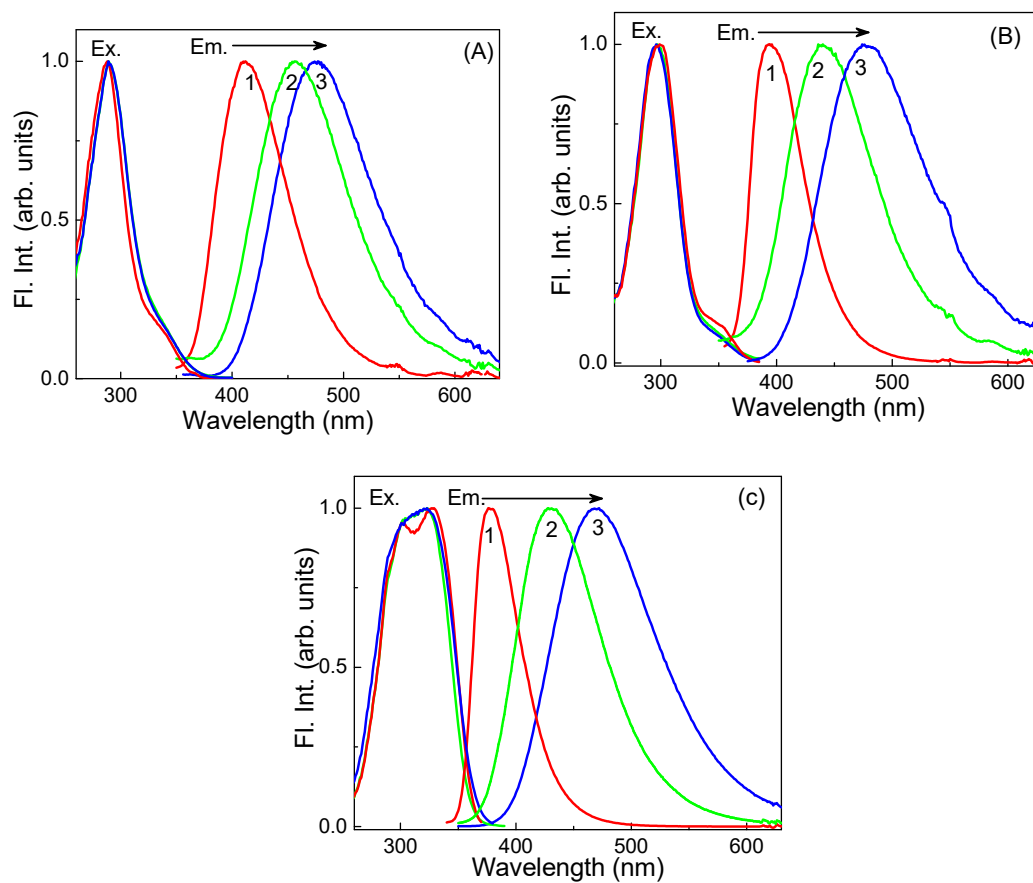
Fig. S2. Peak normalized emission and excitation spectra of TPA-*o* (A), TPA-*m* (B) and TPA-*p* (C) in (1) CH, (2) EA and (3) ACN solvents.
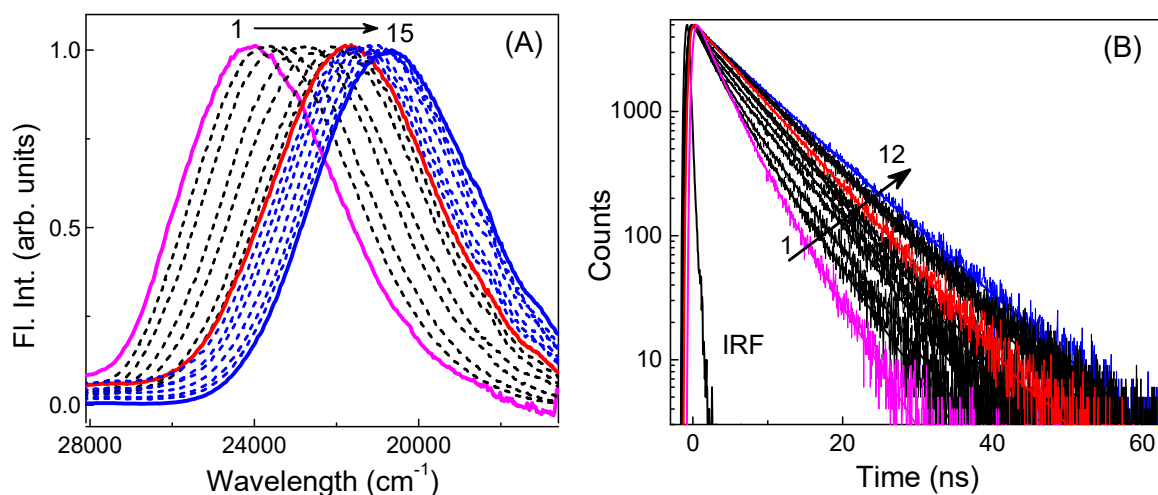
Fig. S3. (A) Peak normalized emission spectra of TPA-*o* in CH (magenta), $CH_{98}EA_2$, $CH_{95}EA_5$, $CH_{85}EA_{15}$, $CH_{80}EA_{20}$, $CH_{60}EA_{40}$, $CH_{40}EA_{60}$, EA (red), $EA_{95}ACN_5$, $EA_{90}EA_{10}$, $EA_{80}ACN_{20}$, $EA_{60}ACN_{40}$, $EA_{40}ACN_{60}$, $EA_{20}ACN_{80}$, ACN (blue) (1-15). (B) Fluorescence decay traces of TPA-*o* in CH (magenta), $CH_{98}EA_2$, $CH_{95}EA_5$, $CH_{90}EA_{10}$, $CH_{80}EA_{20}$, $CH_{60}EA_{40}$, $CH_{20}EA_{80}$, EA (red), $EA_{60}ACN_{40}$, $EA_{40}ACN_{20}$, $EA_{20}ACN_{80}$, ACN (blue) (1-12), monitored at the respective emission maxima in each solvent.

Fig. S4. (A) Peak normalized emission spectra of TPA-*p* in CH (magenta), $CH_{98}EA_2$, $CH_{90}EA_{10}$, $CH_{80}EA_{20}$, $CH_{60}EA_{40}$, $CH_{40}EA_{60}$, $CH_{20}EA_{80}$, EA (red), $EA_{95}ACN_5$, $EA_{90}EA_{10}$, $EA_{80}ACN_{20}$, $EA_{60}ACN_{40}$, $EA_{40}ACN_{60}$, $EA_{10}ACN_{90}$, ACN (blue) (1-15). (B) Fluorescence decay traces of TPA-*p* in CH (magenta), $CH_{98}EA_2$, $CH_{90}EA_{10}$, $CH_{80}EA_{20}$, $CH_{60}EA_{40}$, $CH_{40}EA_{60}$, EA (red), $EA_{95}ACN_5$, $EA_{90}ACN_{10}$, $EA_{80}ACN_{20}$, $EA_{50}ACN_{50}$, ACN (blue) (1-12), monitored at the respective emission maxima in each solvent.

Fig. S5. (A) Peak normalized emission spectra of TPA in CH (magenta), $CH_{90}EA_{10}$, $CH_{50}EA_{50}$, EA (red), $EA_{80}ACN_{20}$, $EA_{50}ACN_{50}$, ACN (blue) (1-7). (B) Fluorescence decay traces of TPA in CH (magenta), $CH_{50}EA_{50}$ (black), EA (red), $EA_{50}ACN_{50}$ (green) and ACN (blue), monitored at the respective emission maxima in each solvent.
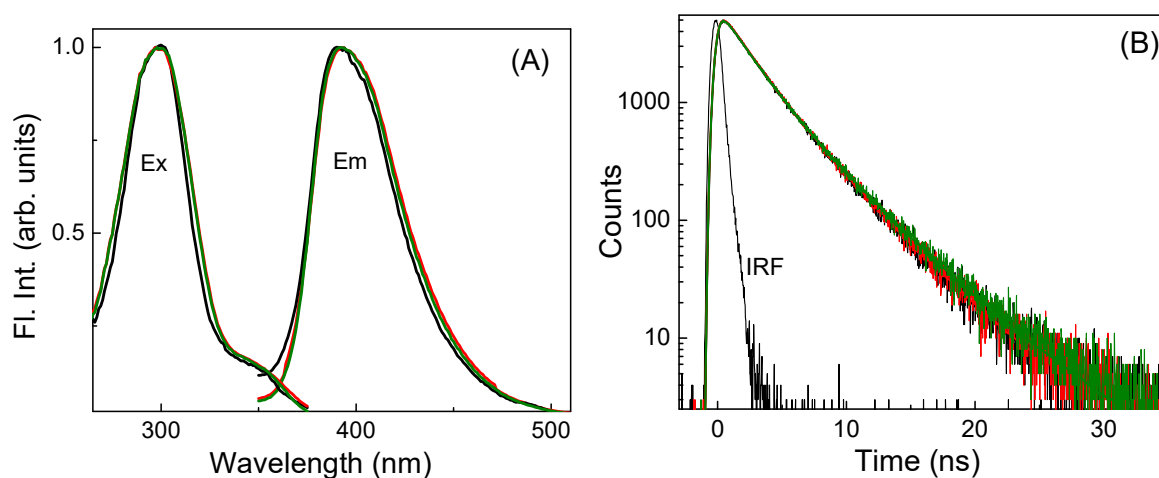

Fig. S6. Fluorescence emission and excitation spectra (A) and decay traces of TPA-*m* in CH at different concentrations of TPA-*m*: 3.5 μM (black), 7.4 μM (red) and 15.3 μM (green).
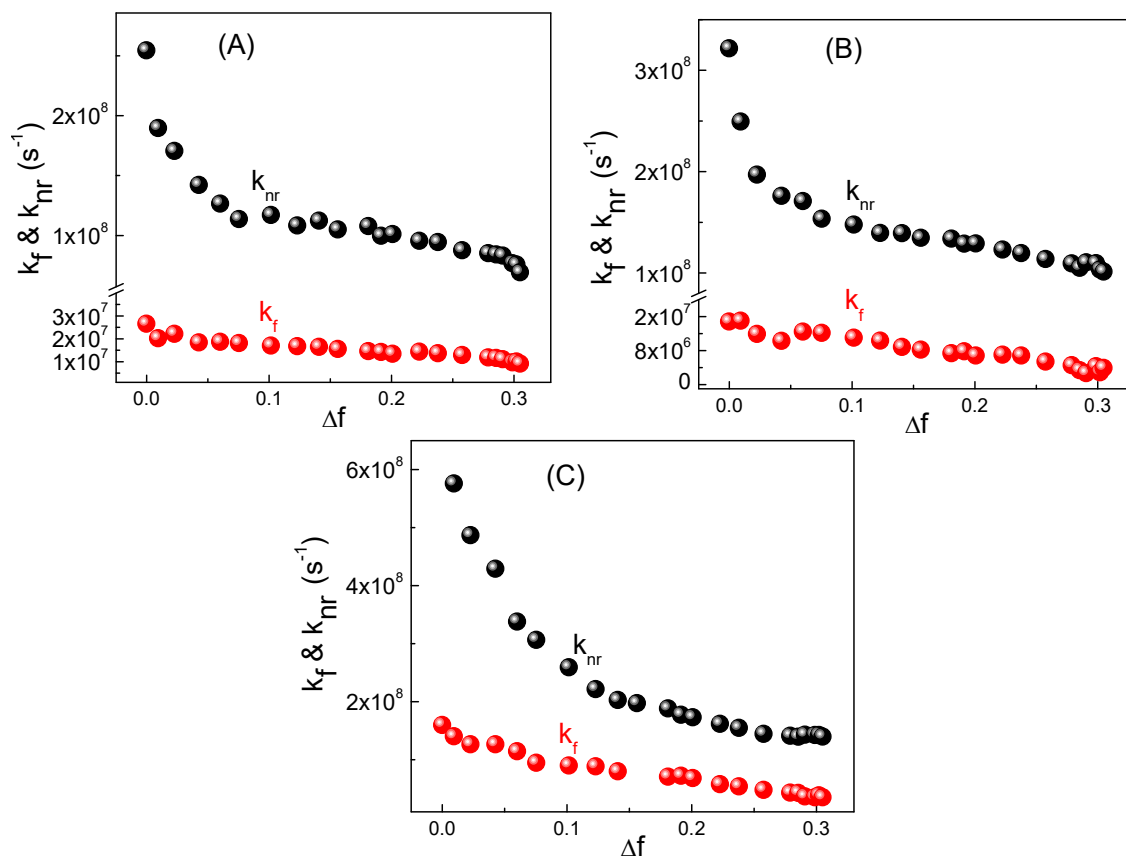
Fig. S7 Plots of radiative (k_f, red) and nonradiative (k_{nr}, black) rates of (A) TPA-*o*, (B) TPA-*m* and (C) TPA-*p*, against the solvent polarity function (Δf).

Note: The radiative (k_f) and nonradiative (k_{nr}) decay rate constants of the dyes were approximately obtained from the measured quantum yields and fluorescence lifetimes (average lifetimes were used for bi-exponential decays) as follows,[2-5]

$$k_f = \frac{\phi_f}{\tau}, \quad k_{nr} = \frac{1 - \phi_f}{\tau}$$

Table S1. Fluorescence decay parameters[a], emission maxima ($\overline{v}_{em}$), quantum yields (ϕ_f), radiative (k_f) and nonradiative (k_{nr}) decay rate constants of TPA-p in solvents of varying polarity parameter (Δf).

Solvent	Δf	τ_1 (ns)	A_1 (%)	τ_2 (ns)	A_2 (%)	$<\tau>$ (ns)	$\overline{v}_{em}$ (cm^{-1})	ϕ_f	k_f ($\times 10^8$) (s^{-1})	k_{nr} ($\times 10^8$) (s^{-1})
CH	0	1.18	100	-	-	1.18	26596	0.190	1.61	6.86
CH$_{98}$EA$_2$	0.009	1.77	51	1.00	49	1.39	26178	0.196	1.40	5.76
CH$_{95}$EA$_5$	0.023	2.09	52	1.14	48	1.63	25773	0.126	1.26	4.87
CH$_{90}$EA$_{10}$	0.043	2.27	60	1.1	40	1.80	25381	0.227	1.26	4.29
CH$_{85}$EA$_{15}$	0.060	2.69	68	1.19	32	2.21	25000	0.253	1.14	3.38
CH$_{80}$EA$_{20}$	0.075	2.91	76	1.16	24	2.49	24691	0.236	0.95	3.07
CH$_{60}$EA$_{40}$	0.123	3.46	91	0.81	9	3.22	24038	0.286	0.89	2.22
CH$_{50}$EA$_{50}$	0.141	3.73	93	0.95	7	3.54	23810	0.283	0.80	2.03
CH$_{40}$EA$_{60}$	0.156	3.78	95	0.59	5	3.62	23753	0.285	0.79	1.97
CH$_{20}$EA$_{80}$	0.181	3.86	100	-	-	3.86	23419	0.273	0.70	1.88
CH$_{10}$EA$_{90}$	0.191	4.01	100	-	-	4.01	23419	0.288	0.72	1.78
EA	0.201	4.14	100	-	-	4.14	23255	0.282	0.68	1.73
EA$_{95}$ACN$_5$	0.223	4.56	100	-	-	4.56	22950	0.262	0.57	1.62
EA$_{90}$ACN$_{10}$	0.238	4.78	100	-	-	4.78	22624	0.260	0.54	1.55
EA$_{80}$ACN$_{20}$	0.258	5.18	100	-	-	5.18	22271	0.250	0.48	1.45
EA$_{60}$ACN$_{40}$	0.279	5.42	100	-	-	5.42	21881	0.233	0.43	1.41
EA$_{50}$ACN$_{50}$	0.286	5.49	100	-	-	5.49	21500	0.234	0.43	1.40
EA$_{40}$ACN$_{60}$	0.291	5.57	100	-	-	5.57	21382	0.203	0.36	1.43
EA$_{20}$ACN$_{80}$	0.299	5.63	100	-	-	5.63	21277	0.198	0.35	1.43
EA$_{10}$ACN$_{90}$	0.302	5.53	100	-	-	5.53	21277	0.212	0.38	1.42
ACN	0.305	5.60	100	-	-	5.60	21278	0.200	0.35	1.41

[a]The fluorescence decays are fitted by considering either single or bi-exponential functions with general expression as, $I(t) = \sum_i a_i \exp(-t/\tau_i)$. The relative contribution of each decay component τ_i, is calculated as, $A_i(\%) = \dfrac{a_i \tau_i}{\sum_i a_i \tau_i} \times 100$ and the average lifetime, $<\tau>$ is calculated as, $\langle \tau \rangle = \sum_i A_i \tau_i / 100$.
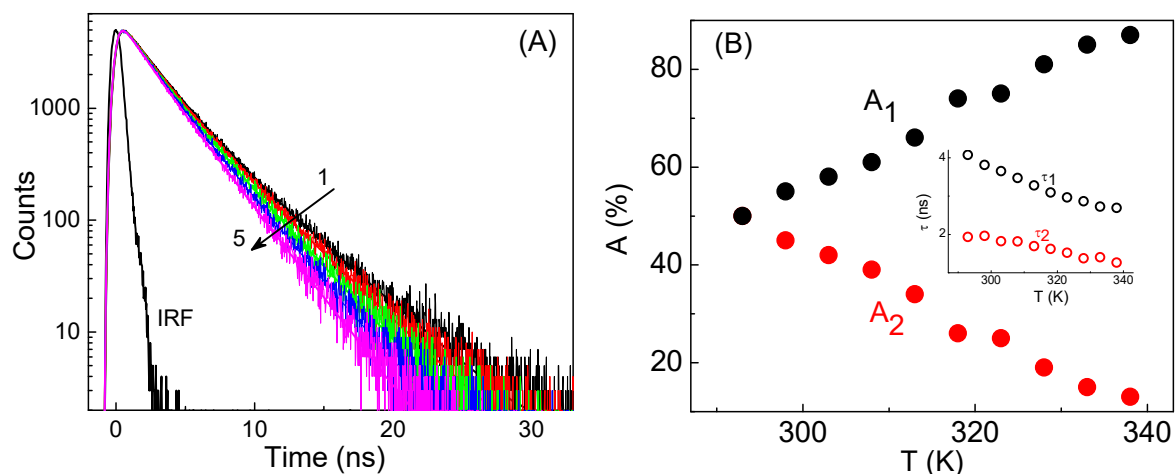
Fig. S8. (A) Fluorescence decay traces of TPA-*m* in CH at 20°C, 30°C, 40°C, 50°C, 65°C (1-5). (B) Plots of the relative contributions (A_1 and A_2) of the two decay components (τ_1 and τ_2) of TPA-*m* in CH against temperature. The variations in the magnitudes of τ_1 and τ_2 with temperature are shown in the inset.
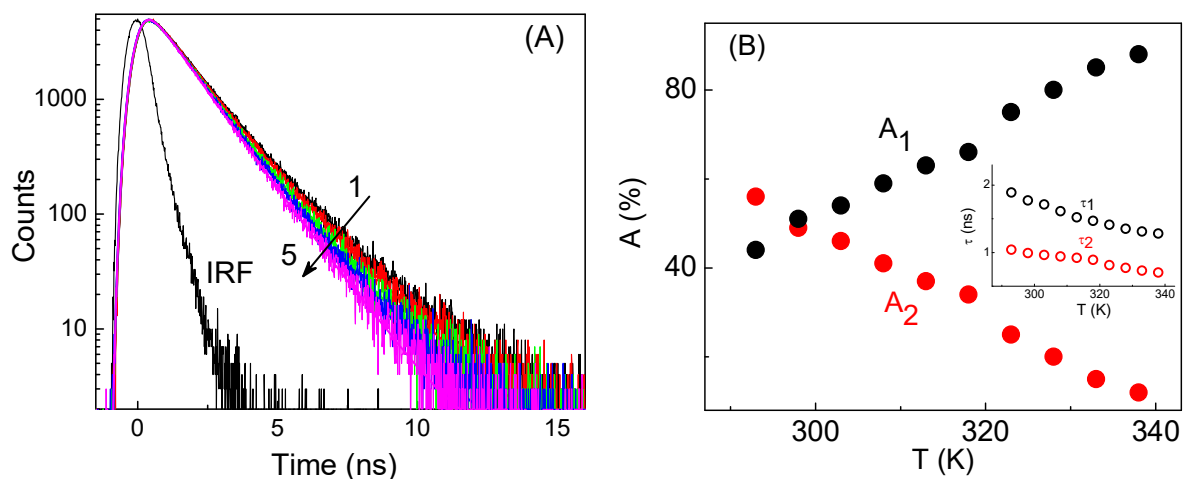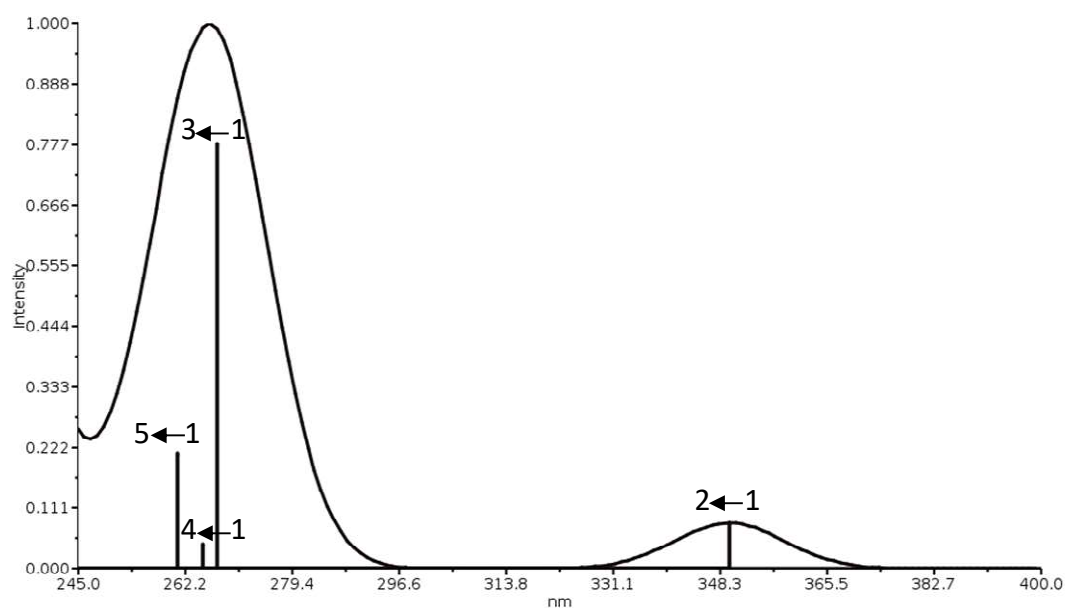

Fig. S9. (A) Fluorescence decay traces of TPA-*p* in $CH_{98}EA_2$ solvent mixture at 20°C, 30°C, 40°C, 50°C, 65°C (1-5). (B) Plots of the relative contributions (A_1 and A_2) of the two decay components (τ_1 and τ_2) of TPA-*p* in $CH_{98}EA_2$ solvent mixture against temperature. The variations in the magnitudes of τ_1 and τ_2 with temperature are shown in the inset.

(A)

(B)

(1) HOMO
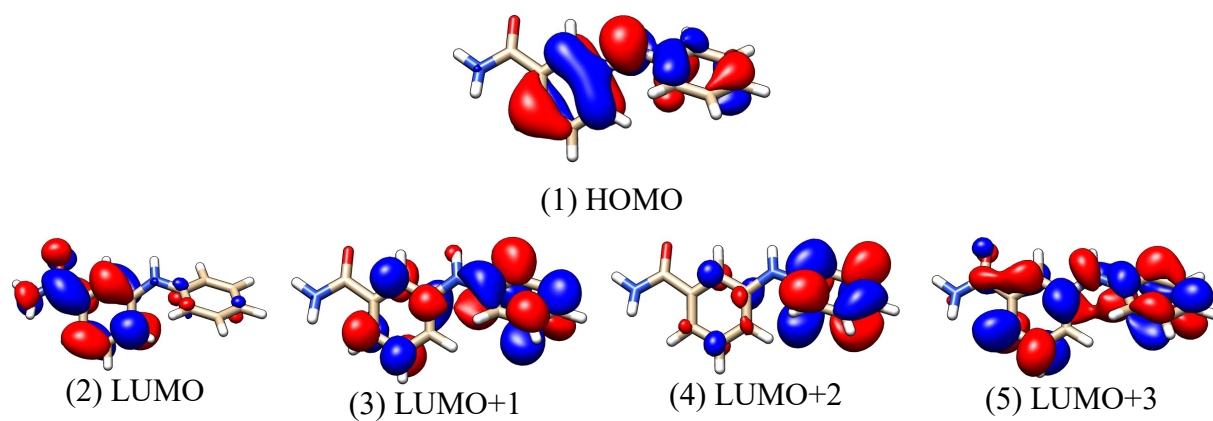
(2) LUMO (3) LUMO+1 (4) LUMO+2 (5) LUMO+3

Fig. S10. (A) Computed absorption spectrum of DPA-*m* dye considering ACN as the solvent medium. (B) Molecular orbitals involved in the four lowest transitions are shown.
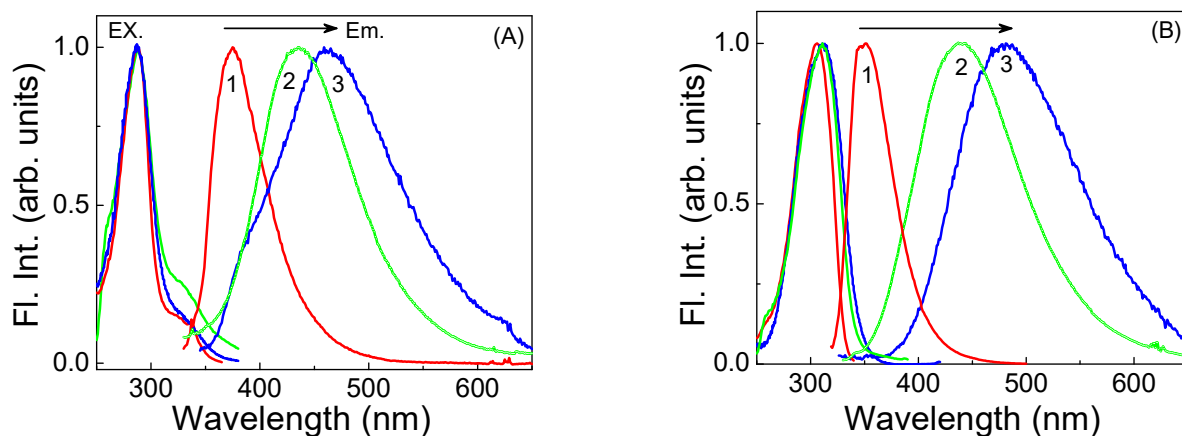
Fig. S11. Peak normalized emission and excitation spectra of DPA-*m* (A) and DPA-*p* (B) in (1) CH, (2) EA and (3) ACN.
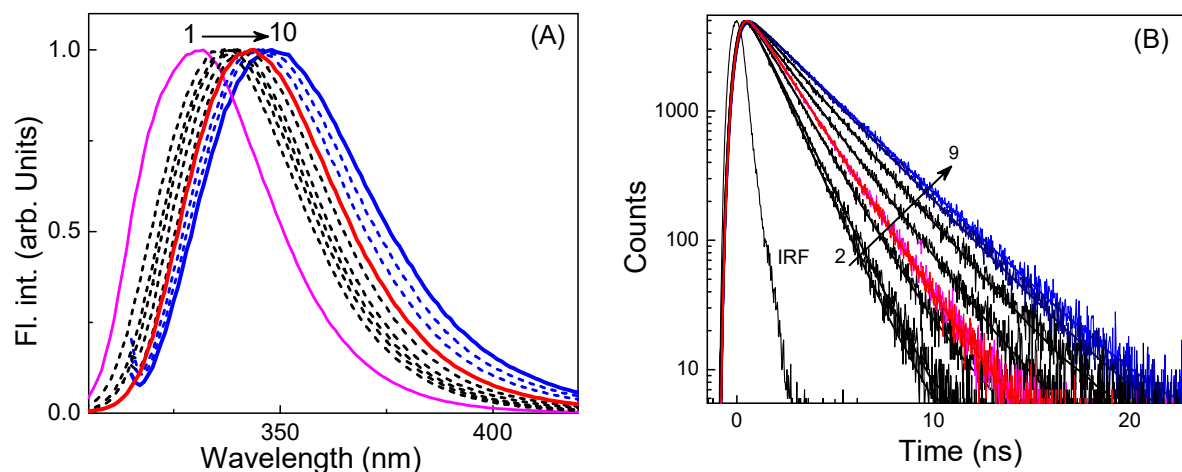

Fig. S12. (A) Peak normalized emission spectra of DPA in CH (magenta), $CH_{98}EA_2$, $CH_{95}EA_5$, $CH_{90}EA_{10}$, $CH_{80}EA_{20}$, $CH_{50}EA_{50}$, EA (red), $EA_{80}ACN_{20}$, $EA_{50}ACN_{50}$, ACN (blue) (1-10). (B) Fluorescence decay traces of DPA in CH (1, magenta), $CH_{90}EA_{10}$, $CH_{80}EA_{20}$, $CH_{50}EA_{50}$, EA (red), $EA_{80}ACN_{20}$, $EA_{50}ACN_{50}$, $EA_{20}ACN_{80}$, ACN (blue) (2-9), monitored at the respective emission maxima in each solvent. IRF is the instrument response function.
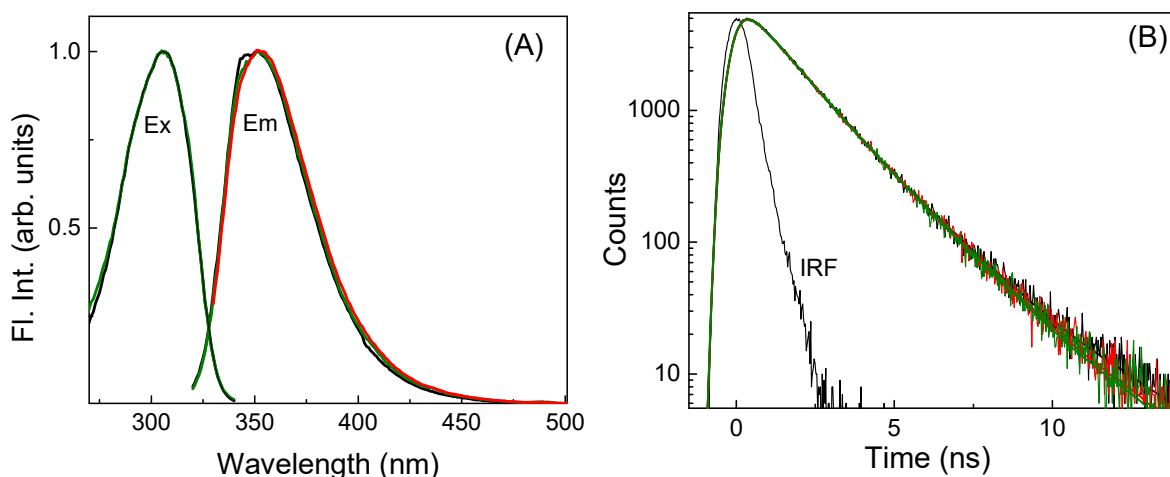
Fig. S13. Fluorescence emission and excitation spectra (A) and decay traces of DPA-*p* in CH at different concentrations of DPA-*p*: 3.8 µM (black), 8.8 µM (red) and 16.5 µM (green).
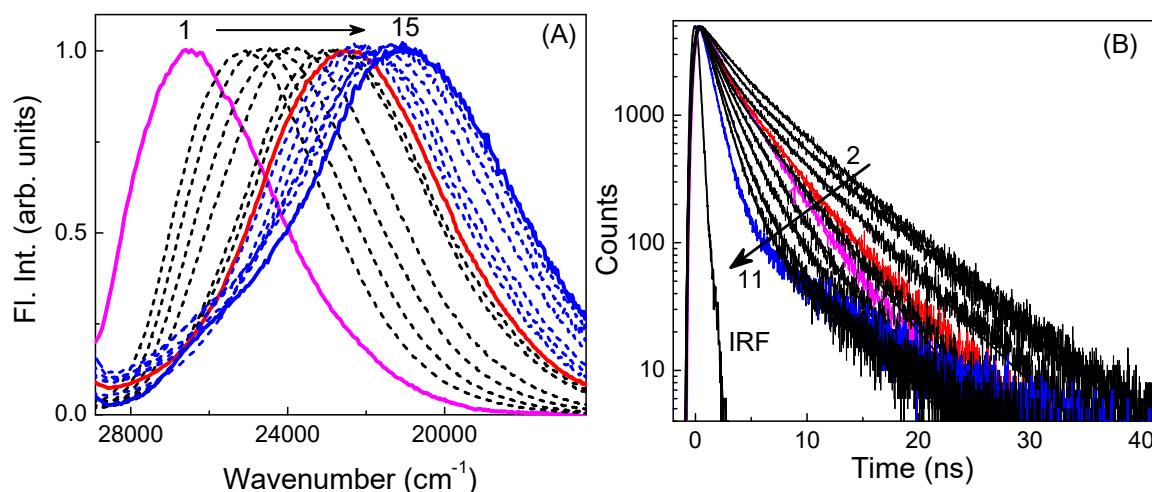

Fig. S14. (A) Peak normalized emission spectra of DPA-*m* in CH (magenta), $CH_{98}EA_2$, $CH_{95}EA_5$, $CH_{90}EA_{10}$, $CH_{80}EA_{20}$, $CH_{60}EA_{40}$, $CH_{50}EA_{50}$, EA (red), $EA_{95}ACN_5$, $EA_{90}EA_{10}$, $EA_{80}ACN_{20}$, $EA_{50}ACN_{50}$, $EA_{40}ACN_{60}$, $EA_{20}ACN_{80}$, ACN (blue) (1-15). (B) Fluorescence decay traces of DPA-*m* in CH (1, magenta), $CH_{99}EA_1$, $CH_{80}EA_{20}$, $CH_{70}EA_{30}$, $CH_{40}EA_{60}$, EA (red), $EA_{90}ACN_{10}$, $EA_{80}ACN_{20}$, $EA_{60}ACN_{40}$, $EA_{40}ACN_{60}$, ACN (blue) (2-11), monitored at the respective emission maxima in each solvent. IRF is the instrument response function.

Table S2. Fluorescence decay parameters[a], emission maxima ($\bar{v}_{em}$), quantum yields (ϕ_f), radiative (k_f) and nonradiative (k_{nr}) decay rate constants of DPA-*m* in solvents of varying polarity parameter (Δf).

Solvent	Δf	τ_1 (ns)	A_1 (%)	τ_2 (ns)	A_2 (%)	$<\tau>$ (ns)	$\bar{v}_{em}$ (cm^{-1})	ϕ_f	k_f (×10^8) (s^{-1})	k_{nr} (×10^8) (s^{-1})
CH	0	3.67	51	1.96	49	2.83	26667	0.037	0.13	3.40
CH$_{98}$EA$_2$	0.009	6.00	59	3.02	41	4.78	25510	0.107	0.22	1.87
CH$_{95}$EA$_5$	0.023	6.03	78	2.82	22	5.33	24938	0.096	0.18	1.70
CH$_{90}$EA$_{10}$	0.043	6.25	68	2.97	32	5.20	24450	0.077	0.15	1.77
CH$_{85}$EA$_{15}$	0.060	6.09	63	2.45	37	4.74	24331	0.071	0.15	1.96
CH$_{80}$EA$_{20}$	0.075	6.09	66	2.08	34	4.72	24155	0.065	0.14	1.98
CH$_{60}$EA$_{40}$	0.123	4.83	70	1.23	30	3.76	23474	0.035	0.11	2.96
CH$_{50}$EA$_{50}$	0.141	3.89	74	1.46	26	3.25	23419	0.032	0.10	2.98
CH$_{40}$EA$_{60}$	0.156	3.87	74	1.16	26	3.17	23202	0.032	0.10	3.06
CH$_{20}$EA$_{80}$	0.181	4.08	74	1.29	26	3.35	23041	0.032	0.09	2.89
CH$_{10}$EA$_{90}$	0.191	4.10	78	1.19	22	3.46	23095	0.032	0.09	2.80
EA	0.201	3.84	74	1.26	26	3.17	22936	0.036	0.09	3.06
EA$_{95}$ACN$_5$	0.223	3.59	67	1.42	33	2.87	22624	0.028	0.08	3.40
EA$_{90}$ACN$_{10}$	0.238	3.33	61	1.40	39	2.58	22472	0.020	0.08	3.80
EA$_{80}$ACN$_{20}$	0.258	3.59	35	1.54	65	2.26	22422	0.016	0.07	4.36
EA$_{60}$ACN$_{40}$	0.279	4.69	15	1.46	85	1.94	22222	0.011	0.06	5.07
EA$_{50}$ACN$_{50}$	0.286	5.20	13	1.33	87	1.83	22124	0.013	0.06	5.39
EA$_{40}$ACN$_{60}$	0.291	5.48	11	1.25	89	1.72	22026	0.007	0.04	5.77
EA$_{20}$ACN$_{80}$	0.299	6.12	11	1.08	89	1.63	21739	0.008	0.05	6.05
EA$_{10}$ACN$_{90}$	0.302	6.24	11	1.01	89	1.59	21692	0.006	0.04	6.27
ACN	0.305	6.45	13	0.94	86	1.62	21645	0.006	0.04	6.17

[a]The fluorescence decays are fitted by considering either single or bi-exponential functions with general expression as, $I(t) = \sum_i a_i \exp(-t/\tau_i)$. The relative contribution of each decay component τ_i, is calculated as, $A_i(\%) = \dfrac{a_i \tau_i}{\sum_i a_i \tau_i} \times 100$ and the average lifetime, $<\tau>$ is calculated as, $\langle \tau \rangle = \sum_i A_i \tau_i / 100$.
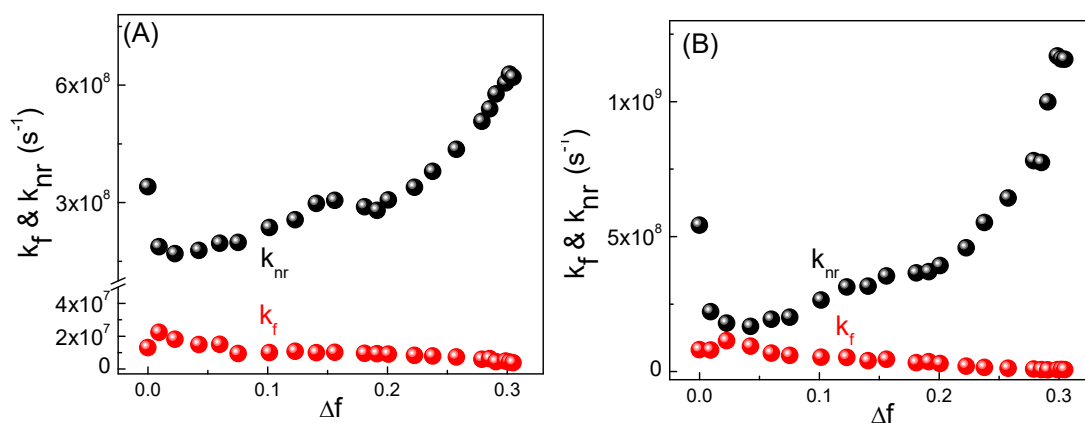
Fig. S15. Plots of radiative (k_f) and nonradiative (k_{nr}) decay rates of (A) DPA-*m* and (B) DPA-*p*, against the solvent polarity function (Δf).
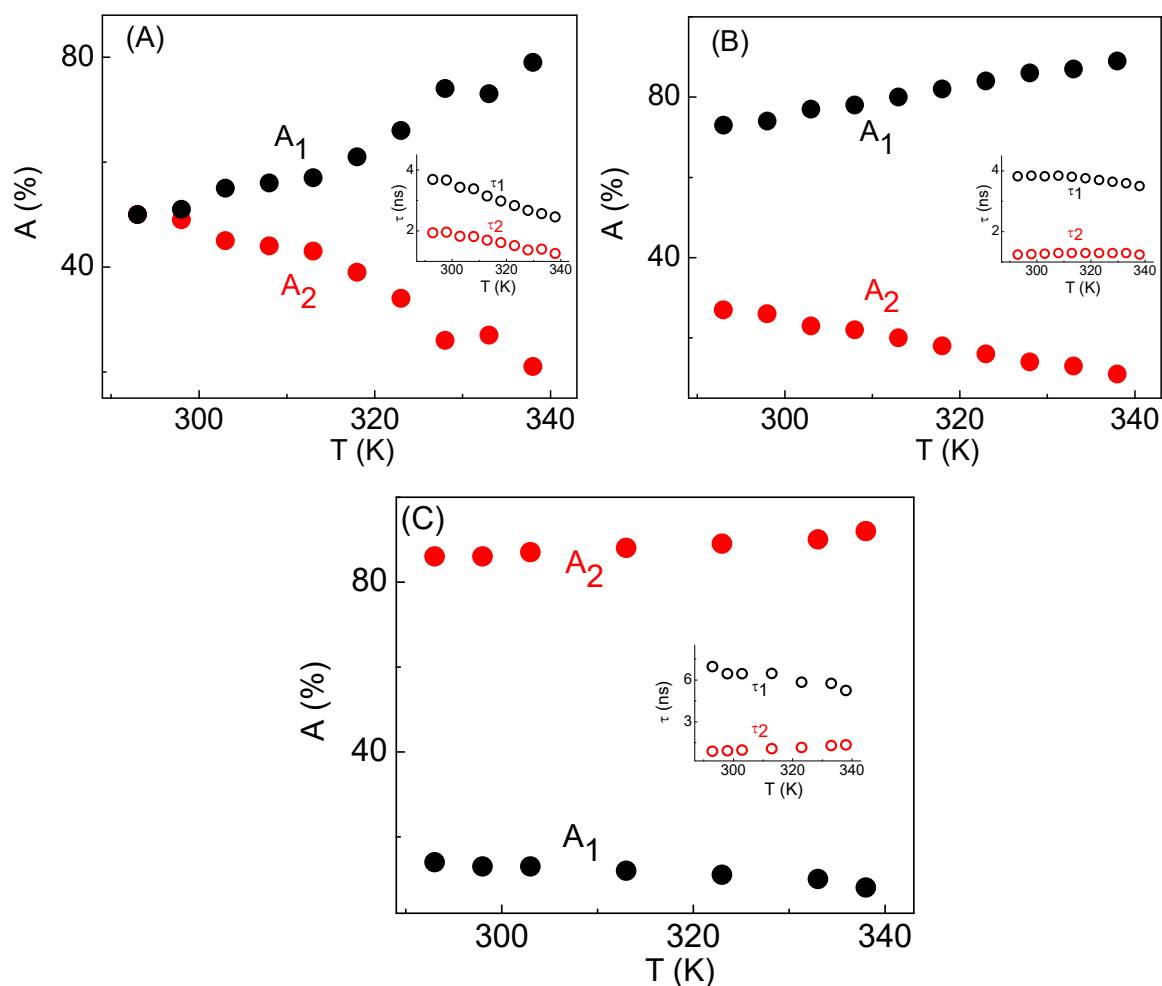

Fig. S16. Plots of the relative contributions (A_1 and A_2) of the two decay components (τ_1 and τ_2) of DPA-*m* against temperature in (A) CH, (B) EA and (C) ACN. The variations in the magnitudes of τ_1 and τ_2 with temperature are shown in the insets.
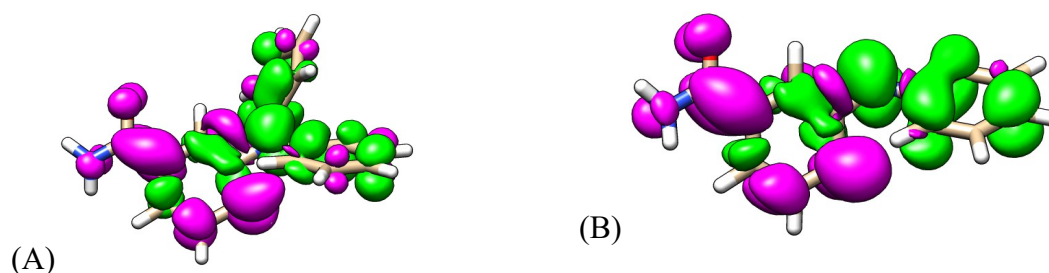
Fig. S17. Difference density plots of the first excited state depicting the HOMO to LUMO transition of (A) TPA-*m* and (B) DPA-*m* in ACN solvent. Green and purple indicate the electron donor and acceptor orbitals.
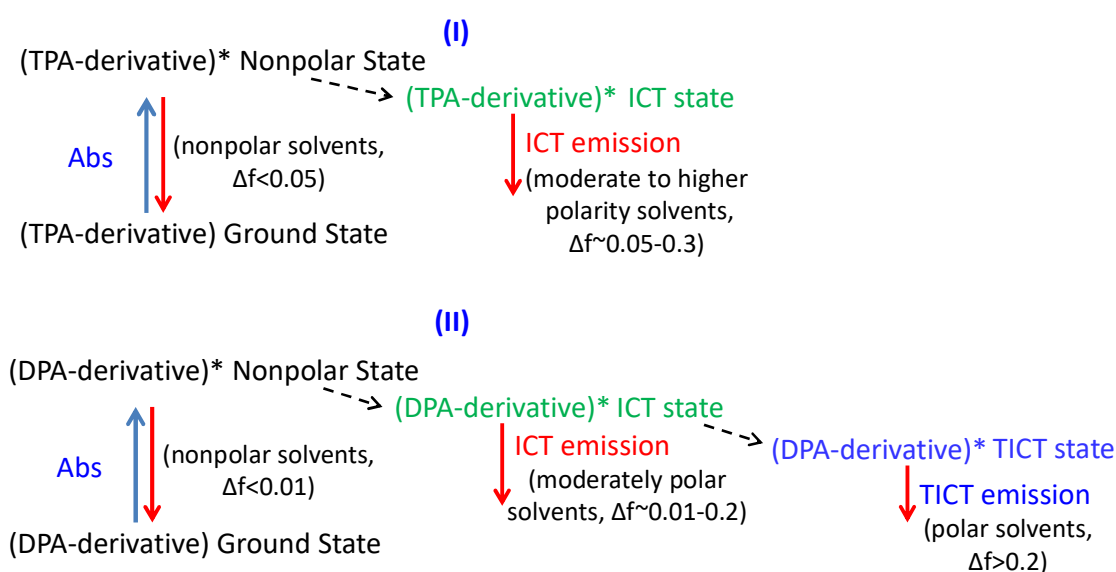

Fig. S18. Schematic representation of the emissive states of (I) TPA and (II) DPA series of dyes in solvents of varying polarities.

References

1   R.S. Meerakrishna and P. Shanmugam, *New J. Chem.* 2019, **43**, 2550-2558.

2   J. R. Lakowicz, *Principles of Fluorescence Spectroscopy*, Springer, New York, 2006.

3   S. Nad and H. Pal, *J. Phys. Chem. A*, 2001, **105**, 1097-1106.

4   J. Cabrera-González, C. Viñas, M. Haukka, S. Bhattacharyya, J. Gierschner and R. Núñez, *Chem. Eur. J.* , 2016, **22**, 13588-13598.

5   A. K. Singh, S. Das, A. Karmakar, A. Kumar and A. Datta, *Phys. Chem. Chem. Phys.*, 2018, **20**, 22320-22330.